Principles and applications of nanofluidic transport

W. Sparreboom*, A. van den Berg and J. C. T. Eijkel

The evolution from microfluidic to nanofluidic systems has been accompanied by the emergence of new fluid phenomena and the potential for new nanofluidic devices. This review provides an introduction to the theory of nanofluidic transport, focusing on the various forces that influence the movement of both solvents and solutes through nanochannels, and reviews the applications of nanofluidic devices in separation science and energy conversion.

Nanofluidics is the study and application of phenomena that involve fluid motion through or past structures with features that measure less than 100 nm in one or more directions. Recent developments in nanofluidics have been driven by the following four factors. First, efforts to replace the polymer gels used for DNA separations with solid-state materials that can be engineered to have structure on the nanoscale[1]. Second, advances in nanofabrication. Third, the availability of new tools to investigate and describe fluid behaviour on the nanoscale, which allow continuum (that is, macroscopic) descriptions to be combined with molecular dynamics (microscopic) descriptions in real devices. Fourth, the prediction of new phenomena at length scales below those that characterize various mechanical and electrochemical phenomena in classical fluids; these new phenomena mostly stem from interactions between the fluid and the walls of the nanofluidic system. Such interactions become important in nanofluidics because of the large surface-to-volume ratios found in these systems.

Although nanofluidics is a reasonably young research field, in the past decade the number of publications in the field has doubled every two years, and recent review articles have discussed the state-of-the-art and speculated about future devices and opportunities[2], discussed the fabrication of nanofluidic devices[3,4,5], and reviewed progress on transport phenomena in general[6] and electrokinetic transport separations in particular[7]. In this article we present a theory that is sufficient for a basic understanding of fluid transport through nanoscale channels, and then review developments in the science and applications of nanofluidic transport.

Theory

Although the discrete nature of individual molecules is evident at the nanoscale, it is still possible to explain the main transport phenomena in nanofluidic systems with a theory based on continuum and mean-field approaches. This is possible because the results obtained with this approach are similar to those obtained from models that treat the molecules as discrete particles, with the differences being limited to the behaviour of the few layers of molecules closest to the wall of the nanochannel[8]. Transport through smaller (often non-permanent) pores, such as occurs in reverse osmosis membranes, is better described by the solution–diffusion model[9]. (Different modelling techniques are reviewed in ref. 10.)

The transport of solutes and solvent through nanochannels or nanopores depends on three factors. First, the presence of external forces, such as an electrical potential gradient or a pressure gradient: these forces are needed to drive transport along the nanochannel. Second, the presence of various colloidal forces, which lead to a variation in the solute concentration across the nanochannel (Table 1). Third, the presence of friction forces between the wall and the solvent, and also between the wall and the solute molecules. The solute and solvent transport fluxes can be deduced from knowledge of these three forces. The same approach has previously been used to describe transport in biological systems, such as the kidneys[11], and was further developed by researchers in separation science[12,13] and membrane technology[14].

Solute concentration distribution. We treat both small ions and larger colloidal particles with sizes 1–100 nm in a single theoretical framework. Both these solutes are attracted to or repelled from the nanochannel wall by colloidal forces[15] that act over distances ranging from less than 1 nm to more than 100 nm. As almost all wall materials carry surface charge, there is often an electrostatic force that repels ions with the same charge as the wall (co-ions) and attracts ions with the opposite charge (counter-ions). However, all the counter-ions do not end up against the wall: instead, the homogenizing action of the thermal (Brownian) motion results in an electrical double layer adjacent to the wall, with an increased concentration of counter-ions and a decreased concentration of co-ions (Fig. 1). The simultaneous screening action of all the ions means that the electrical potential in the double layer decays as $\exp(-y/\lambda)$, where y is the distance from the wall and λ is the Debye screening length. (λ is inversely proportional to the square root of the ionic strength: $\lambda \approx 0.7$ nm at the physiological ionic strength of 150 mM, and ≈ 10 nm in a 1 mM solution.)

Van der Waals forces have the longest range of all the colloidal forces and have a typical interaction length of 10 nm. Figure 2 shows the interaction potential experienced by a nanoparticle when the two dominant forces are the electrostatic and van der Waals forces[15]. Another force that is often important in nanofluidics, especially in biological systems, is the hydrophobic attraction, which is caused by a number of different mechanisms with ranges of a few nanometres up to 100 nm (refs 16,17). The hydrophobic interaction is much stronger than the van der Waals forces over short distances, and decays exponentially with a decay length of ~2 nm. The hydrophobic interaction also has an important role in protein adsorption[18].
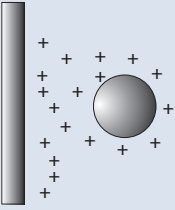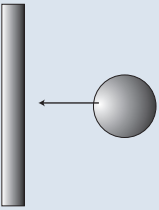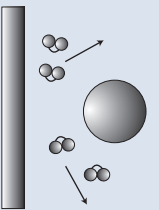
We can formulate an interaction potential for all these forces, and Table 1 shows these for interactions between a planar surface and a spherical particle, and a planar surface and a small ion. Assuming that these interactions are additive, we can write an interaction potential $E(y)$ that sums and time-averages all solute–wall interactions. As a result of the combined action of the forces and the thermal energy, the solute concentration $c(y)$ can be written as

$$c(y) = c_0 \exp(-E(y)/kT) \qquad (1)$$

BIOS/Lab on a Chip group, MESA+ Institute for Nanotechnology, University of Twente, PO Box 217, 7500 AE Enschede, The Netherlands.
*e-mail: w.sparreboom@utwente.nl

Table 1 | Free energies between a plane and a particle or ion.

Interaction potential	Between particle and plane	Between small ion and plane
Electrostatic	$E_{el} = \varepsilon\psi^2 r \exp(-y/\lambda)$	$E_{el} = zq\psi\,\exp(-y/\lambda)$
Lifshitz-van der Waals	$E_{vdw} = -\dfrac{Ar}{6y}$	
Hydrophobic interaction	$E_{hp} = -CD_0 r \exp(-y/D_0)$	

Approximate expressions for the free energy (E) of the colloidal interaction between a negatively charged spherical particle of radius r and a planar surface (left), and a small ion of charge $+zq$ and a planar surface (top right) as a function of the distance y between the particle (or ion) and the surface. See ref. 102 for more details. ψ, electrical surface potential of surface and spherical particle; λ, Debye screening length; ε, medium dielectric constant; A, Hamaker constant ($A = 6\times10^{-21}$ J for the interaction between a protein and a synthetic polymer surface in water[18,103]); C and D_0 are constants ($C \gg 0.4$ N m^{-1}; $D_0 \gg 2$ nm. See ref. 16).

where c_0 is the concentration in the bulk (where solute–wall forces are absent and the interaction potential is zero), K is the Boltzmann constant and T is the temperature.

A process called Born repulsion or steric hindrance, which is caused by the overlap of molecular electron clouds, also prevents the solutes from approaching the wall too closely. For a spherical particle, the distance of closest approach is equal to its radius.

Depending on many different factors (including the charge on the solute, the charge on the wall and the nature of the solvent), the solute can be repelled from the wall, it can experience a superficial energy minimum at some distance from the wall (Fig. 2), or it can experience a deep energy-minimum close to the wall. Figure 1 shows $c(y)$ (also known as Boltzmann distribution profiles) for two different systems: salt ions in a nanochannel in which the electrical double layers at each wall overlap (Fig. 1a); and large solute particles in a nanochannel with strong colloidal forces and steric hindrance (Fig. 1b).

Solute partitioning. Owing to the colloidal forces mentioned above, the average solute concentration inside the nanochannel $\langle c \rangle$ is different to the concentration in bulk solution c_0. The ratio between both, $\Phi \equiv \langle c \rangle/c_0$, is called the solute partition coefficient and can be found by integrating the Boltzmann distribution profile (equation (1)) between the limits allowed by the Born repulsion. For a spherical solute of radius r in a nanochannel with a width of $2h$, we obtain:

$$\Phi = \frac{\langle c \rangle}{c_0} = \frac{1}{h}\int_0^{h-r} \exp(-E(y)/kT)\,dy \qquad (2)$$

When E is the electrostatic interaction potential, Φ gives a measure of the ion permeability–selectivity (permselectivity) of the pore. If the Debye length is comparable to h, the double layers at both walls will overlap and the nanochannel will mainly be occupied by counter-ions (Fig. 1a). When only steric exclusion occurs ($E(y) = 0$), we find that $\Phi = (1 - r/h)$.

Non-spherical solutes[19] have to sacrifice rotational freedom to enter the channel, and if they are (semi)flexible like DNA, they must also sacrifice conformational freedom. This will come at an entropic energy cost which can greatly reduce Φ depending on the macromolecular size[20].

Solvent transport. In nanochannels, solvent can be transported by an axial pressure gradient (hydrodynamic flow) and/or an axial electrical potential gradient (electro-osmotic flow). The average solvent velocity $\langle v_S \rangle$ is obtained by superimposing both velocity profiles and averaging across the channel[21]:

$$\langle v_S \rangle = \frac{1}{h}\int_0^h v_S(y)\,dy = \frac{1}{h}\int_0^h \left(\underbrace{\frac{1}{2\eta}\left(y^2 - 2hy\right)\frac{dP}{dx}}_{\text{Hydrodynamic flow}}\right)dy$$
$$+ \frac{1}{h}\int_0^h \left(\underbrace{\frac{\varepsilon}{\eta}\left(\zeta - \psi(y)\right)\frac{d\phi}{dx}}_{\text{Electro-osmotic flow}}\right)dy \qquad (3)$$

where dP/dx is an applied pressure gradient, ζ is the electrical potential at the plane of shear (this plane, which is parallel to the wall, is the first plane of molecules that are moving rather than adsorbed to the wall), $\psi(y)$ is the electrical potential in the double layer, $d\phi/dx$ is an applied axial electrical-potential gradient, η is the solution viscosity and ε is the permittivity of the solution. We find that hydrodynamic pumping is problematic in nanofluidics because the average velocity is proportional to h^2, so it becomes very small for nanochannels. Electro-osmotic pumping, on the other hand, remains viable in nanofluidics because the electro-osmotic flow velocity only markedly decreases when double-layer overlap occurs and $\phi(y)$ approaches ζ (ref. 21). The hydrodynamic flow profile is parabolic (as in larger channels), whereas the electro-osmotic flow profile follows the profile of the electrical potential ($\zeta - \phi(y)$) across the channel. In nanochannels with double-layer overlap, the electro-osmotic flow profile thus approaches a parabolic shape, whereas in larger channels the velocity increases steeply near the channel walls and maintains a constant value for the remainder of the channel width to give a 'plug' profile[21].

Solute transport. Solutes can be transported by solvent transport (convection), by a solute concentration gradient (diffusion) or, for ions, an electrical potential gradient (migration). The solute fluxes resulting from these three driving forces are combined in
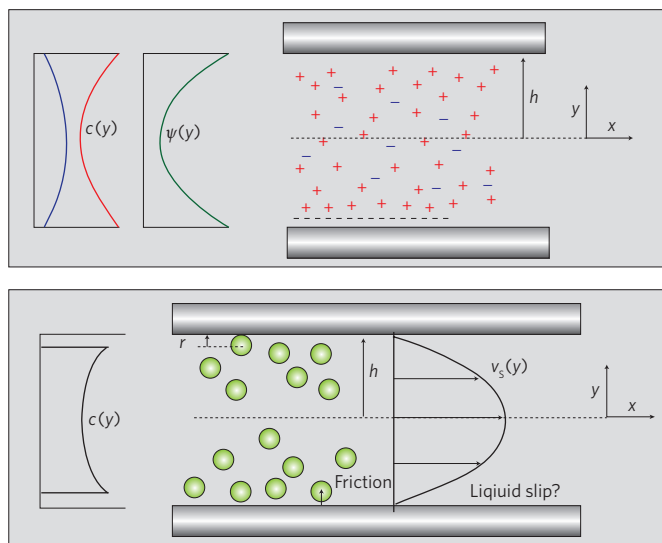
Figure 1 | Concentration and velocity profiles in a nanochannel. a, The concentrations of positive (red line) and negative (blue line) salt ions vary with position y in a nanochannel of width $2h$. The walls are negatively charged so the concentration of positive ions (the counter-ions in this system) is highest near the walls and lowest in the middle of the channel. The total electrostatic potential inside the nanochannel (green line) also varies with y. In this example the electrical double layers formed at each wall (see main text) overlap, which results in the nanochannel being occupied mostly by counter-ions. **b**, The concentration profile (left) for large solute particles of radius r attracted to the wall by colloidal forces, but excluded by steric hindrance. In convection-driven solute transport, the solute flux J is the product of the concentration profile $c(y)$ and the velocity profile $v_s(y)$ (thin black line) of the solvent flow. The maxima in $c(y)$ are close to the walls, while the maximum of $v_s(y)$ is in the centre of the nanochannel. Hydrodynamic friction between the large solutes and the wall also influences the solute flux, and liquid slip at the walls sometimes influences the flux.

the Nernst–Planck equation. This equation can be formulated for nanochannel transport to give[11,14]:

$$\langle J \rangle = \frac{1}{h}\int_0^h \underbrace{(c(y)\,v_s(y))}_{\text{Convection}}\mathrm{d}y - \frac{1}{h}\int_0^h \underbrace{\left(\mathrm{D}_\infty \frac{\mathrm{d}c(y)}{\mathrm{d}x}\right)}_{\text{Diffusion}}\mathrm{d}y$$

$$- \frac{1}{h}\int_0^h \underbrace{\left(\frac{zq\mathrm{D}_\infty}{kT}\,c(y)\,\frac{\mathrm{d}\phi}{\mathrm{d}x}\right)}_{\text{Migration}}\mathrm{d}y \qquad (4)$$

where $\langle J \rangle$ is the area-averaged solute flux, D_∞ the diffusion coefficient in free solution and zq is the ionic charge. This equation differs from the bulk transport equation because the colloidal interactions between solute and wall mean that it is necessary to include the effects of the concentration profile $c(y)$. Sometimes it is also necessary to add hydrodynamic friction (see below) to this equation.

Charge transport. Hydrodynamic flow through a channel with a charged surface (Fig. 1a) transports the electric charge in the double-layer region downstream. This electrical current, which is called the streaming current, generates an axial electrical field that subsequently causes a backflow of current. In the steady state, both currents are equal and the resulting potential difference over the channel is called the streaming potential. In nanochannels, this
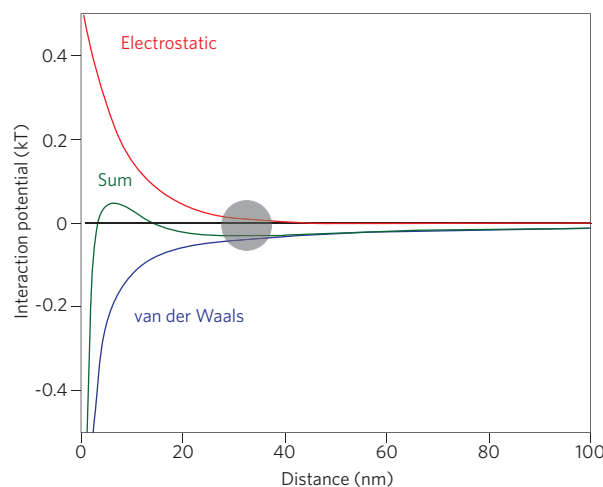
streaming potential causes an appreciable electro-osmotic backflow in pressure-driven flow (see equation (3)), seemingly increasing the viscosity (the electroviscous effect)[22].

Friction. Two sources of friction are important in nanofluidics: solvent–wall interactions and hydrodynamic solute–wall interactions. The hydrophobic interaction can lead to a lower density of water molecules in the layers adjacent to a hydrophobic wall[17], which means that the water–wall interactions decrease and water will partly slip past the wall, giving a non-zero wall velocity. This 'liquid slip' is quantified by the slip length b (ref. 23), and slip lengths of 20–50 nm have been reported for hydrodynamic flow experiments on hydrophobic surfaces[24]. Theoretically, liquid slip increases the hydrodynamic flow velocity in a nanochannel by a factor of $(1 + 6b/h)$, and the electro-osmotic flow velocity by a factor of at least $(1 + b/\lambda)$ (ref. 25).

To account for the frictional effects of solute–wall interactions, equation (4) is generally modified by dividing the terms for convection, diffusion and migration with 'hindrance factors'. Expressions for these coefficients have been derived for a few simple solute and channel geometries[11,14].

Entrance and exit processes. In general the solute flux (mol m^{-2} s^{-1}) in a nanochannel will differ from the flux in bulk solution owing to difference in average concentration given by Φ in equation (2). As a result solute depletion and enrichment occurs at the channel openings, a phenomenon called concentration polarization (Fig. 3). This phenomenon is often a problem, but it can also be exploited in applications. Concentrated solutes can, for example, block the channel (causing fouling in membranes), and increased salt concentrations can decrease the channel ion-permselectivity, as the Debye length is a function of the ionic strength. However, concentration enhancements can be useful in chemical analysis and electrodialysis, as we shall see below.

Applications in solvent transport

The prediction[25] that liquid slip will strongly enhance the magnitude of electro-osmotic flow in nanochannels recently received support from experiments that found that the electro-osmotic flow

Figure 2 | Interaction potential between a particle and a surface (both negatively charged). The nanoparticle (grey circle) is attracted to the surface by van der Waals forces (blue line), but repelled by electrostatic forces (red line), and is shown here at the minimum of the combined potential (green line). $r = 5$ nm; $\psi = -25$ mV; $A = 6\times10^{-21}$ J; $\varepsilon = 80 \times 8.9\times10^{-12}$ F m^{-1}; $\lambda = 10$ nm. The hydrophobic interaction is not considered. In DLVO theory[15] (named after Derjaguin, Landau, Verwey and Overbeek) the (in)stability of colloid solutions can be explained by a combination of van der Waals forces and electrostatic forces.
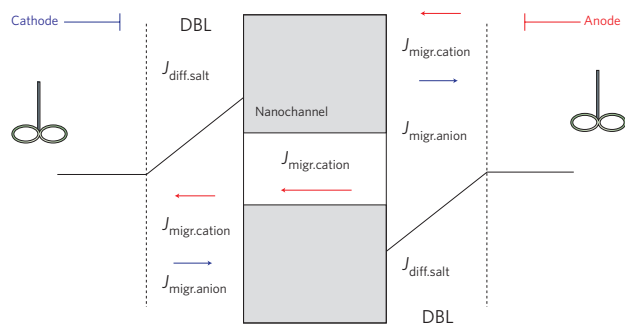
Figure 3 | Concentration polarization. When an electrical current is sent through a nanochannel that presents different permeabilities to anions and cations, the phenomenon of concentration polarization can be observed. In both regions outside the nanochannel, migrational current is carried by cations ($J_{migr.cation}$) and anions ($J_{migr.anion}$), whereas inside the nanochannel current is mainly carried by the counter-ions (which are cations in this case). Since the transport rate of cations inside the nanochannel is approximately twice as high as outside, the concentration of cations is depleted at the anode and enriched at the cathode. Because of the need to maintain electrical neutrality the amount of cations at both ends is matched by the amount of anions, which causes a gradient in salt concentration in the so-called diffusion boundary layers (DBL) on both ends of the nanochannel. This in turn causes a diffusional flux of salt ($J_{diff.salt}$) from the cathode side and towards the anode side. The propellers on both sides indicate that fresh solution is available at large distances from the nanochannel and that bulk parameters apply at these distances. Adapted from ref. 6 with permission © 2008 APS.

velocity increased by a factor of two at hydrophobic surfaces[26,27]. Other experiments reported that the current increased by a factor of 20–50 when a positive gate voltage was applied to 20 x 30 nm silica nanochannels[28], which is thought to be due to liquid slip caused by the perpendicular field.

There have been relatively few experiments on pressure-driven flow in nanochannels for the reasons discussed above, and these have mostly focused on the use of streaming currents to generate electric power[29–31] or study the behaviour of DNA molecules in nanopores[34]. Of particular note are two reports of enormous enhancements (by four orders of magnitude) of pressure-driven flow in carbon nanotube membranes, possibly caused by liquid slip[33,34].

Several other driving forces have been proposed in literature[35–39]. In diffusio-osmosis[39–42], for example, liquid transport is generated by a difference in solute concentration at the two ends of the channel. Its origins lie in the attraction of solute molecules to the wall, which causes a locally high solute concentration, which in turn generates an osmotic pressure gradient at the channel wall in the same direction as the solute concentration gradient. This osmotic pressure gradient finally generates liquid flow. However, the flow velocities are ~μm s^{-1}, which is probably the reason that diffusio-osmosis has received less attention than electro-osmosis, although this could change if experiments can confirm the prediction[43] that the introduction of liquid slip would increase the flow velocity by a factor b/L_m, where L_m is the molecular length scale. It was predicted that this factor could be as high as 100.

Flow can also be driven by a process called pervaporation (which is partial evaporation through a membrane). Flow rates of up to 70 μm s^{-1} driven by pervaporation have been reported for a 500-nm-high polyimide channel with a thin 'roof'[35]. The pervaporation induces fluid flow by moving water from the high chemical potential in the channel below the roof to the low chemical potential in the atmosphere above the roof (as happens in trees). Ref. 35 also reports fluid flow induced by osmosis on the same device: in
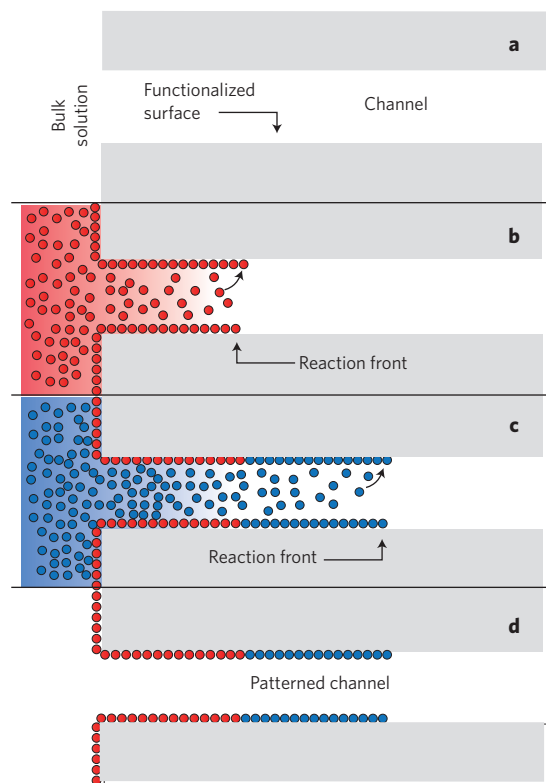

Figure 4 | Diffusion-limited patterning. a, When a bulk solution can only enter a nanochannel (with a functionalized surface) from one end, it is possible to pattern the surface by subsequent introduction of multiple reactants with a technique known as diffusion-limited patterning. **b**, When a reactant (red) is introduced into the bulk solution for a certain length of time, it diffuses into the channel and binds to the surface, forming a well-defined reaction front. **c**, When a second reactant (blue) is introduced, it reacts with the region of the channel beyond the first reactant. **d**, Repeating this process with different reactants results in patterning of the reactants inside the channel. Adapted from ref. 51 with permission © 2006 ACS.

this case water moves from a region of low salt concentration to a region of high salt concentration. These pumping techniques exploit the large surface-to-volume ratios in nanochannels. Pumping by evaporation at one or multiple channel exits has only been demonstrated in microchannels so far, but it should also be possible with nanochannels[44,45].

It is also possible to drive liquid through a nanochannel with flexible walls by deforming the nanochannel[37,46]. Nanochannels have been created in polydimethylsiloxane (PDMS) by applying mechanical stress to thickly oxidized PDMS layers. The stress produces cracks with triangular cross-sections and controllable widths and heights (of 688 and 58 nm respectively in ref. 46). The combination of this shape and the use of extra-stiff PDMS probably prevent the walls of the nanochannel sticking to each other in an irreversible manner. Liquids can be pumped through these channels by applying a relatively small pressure (22–42 kPa) to the PDMS; lower pressures can be used to control the flow velocity and higher pressures can completely close the channels. The potential for massive parallelization offered by these techniques, combined with the relative ease of fabrication, means that their impact on nanofluidics could match that of a similar technique in microfluidics[47].

All other techniques exploit the dominance of surface tension and viscous forces over inertia in nanofluidic channels. Capillary filling[38] is one technique that could potentially be scaled down in size from the micro- to the nanoscale. Pumping is performed by
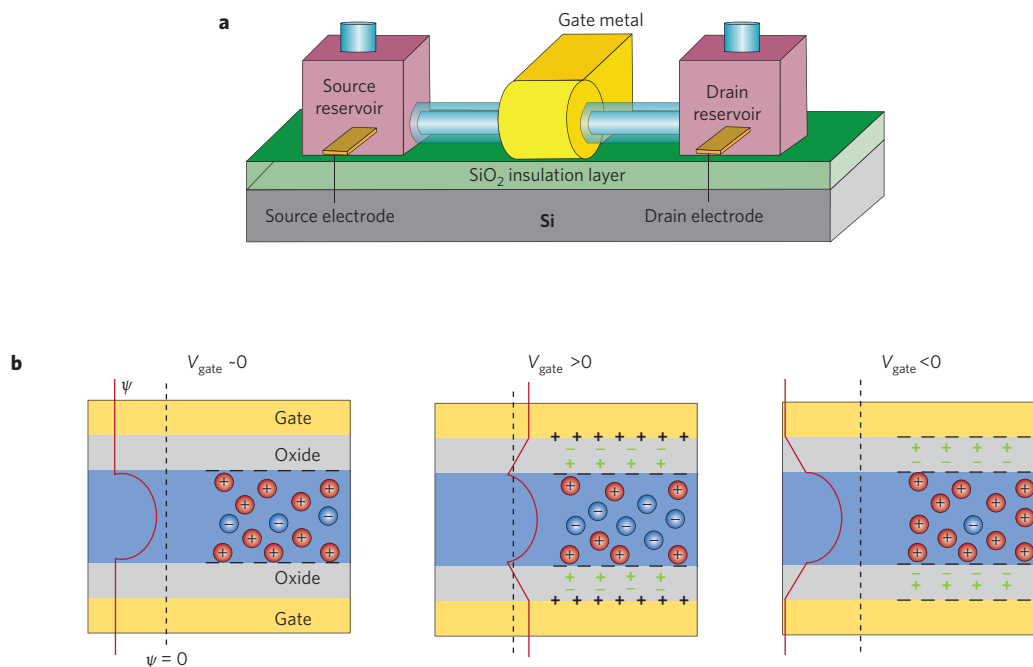
Figure 5 | The nanofluidic transistor. a, Schematic of a nanofluidic field-effect transistor. In a conventional field-effect transistor, the current flowing through the channel between the source and drain electrodes is driven by the voltage applied across these electrodes, and it can be controlled by applying a voltage to the gate electrode. The voltage on the gate electrode essentially modulates the type (that is, electrons or holes) and number of charge carriers in the semiconductor channel below it (ref. 104). In a nanofluidic transistor the flow through a nanochannel can be driven by pressure, an applied electric field or a concentration difference. By applying a bias voltage between the gate electrode and the solution, the wall potential can be changed, modulating the counter-ionic charge in the solution. **b**, When the gate voltage (V_{gate}) is zero, the electrostatic potential ψ (red line) does not vary with position in the oxide, but it decays exponentially to a minimum in the centre of the channel (shown in blue; ψ is positive to the left of the line showing $\psi = 0$). In this example the walls have a negative surface charge (black symbols) and the electrical double layers at each wall almost meet in the centre of the channel, so the channel is mostly occupied by counter-ions (which are positive in this system). For $V_{gate}>0$ the electrostatic potential at the wall becomes less negative, effectively decreasing the transport rate of the positive ions (or even strongly increasing the transport rate negative ions for a high V_{gate}). This results in a positive wall because the applied voltage polarizes the oxide layer, which can be represented by a positive surface charge (green symbols) on one side and a negative surface charge on the other, with ψ decaying linearly within the oxide layer. For $V_{gate}<0$ the electrostatic potential at the wall becomes more negative, increasing both the number and transport rate of positive ions. Adapted from ref. 84 © 2005 ACS.

a repetitive cycle in which a water plug is replaced with gas (by inducing a slight gas over-pressure), and then again the gas plug is replaced with water (by capillary pressure). A structural asymmetry in the system thereby provides directionality to the pumping.

A more exotic way of exploiting surface tension and viscous forces is to induce liquid flow in a lipid nanotube between unilamellar vesicles[36]. This is done by using a micromanipulator to continuously change the shape of one of the vesicles, which also changes the surface tension: lipid then flows from regions of high surface tension to regions of low surface tension in the nanotube, and the liquid in the nanotube is dragged along by viscous forces.

Applications in solute transport
We have seen that solute transport in nanochannels is strongly influenced by colloidal interactions with the wall, and these interactions can significantly reduce the solute transport velocity, which is a disadvantage for most applications (although it is essential in liquid chromatography[48]). In this section we will discuss the influence of adsorption (both reversible and irreversible), electrostatic forces, steric exclusion and friction on solute transport, and also discuss the active control of transport, entrance and exit effects, and how to deal with low detection limits in nanofluidic systems.

The influence of adsorption. A number of recent experiments have explored how the transport of molecules (mostly cationic molecules) is modified in nanochannels[49–54]. When adsorbing molecules diffuse through a nanochannel, the reduced transport rate is accompanied by a sharp diffusion front. In the case of reversible adsorption the diffusion coefficient is reduced to $D_\infty/(R + 1)$, where R is the concentration ratio of immobilized and free solute[55].

Irreversible adsorption of, for example, proteins can be used to pattern the surface of microfluidic and nanofluidic channels[51,56] (Fig. 4). The diffusion constants measured for protein and positively charged dyes can be between four[50] and eight[49] orders of magnitude lower than the bulk values, making it practically impossible to use such molecules as tracers in measurements of the flow velocity. (See ref. 51 for a simple expression for the effective diffusion coefficient in the case of irreversible adsorption).

The influence of electrostatic forces. As mentioned above, the electro-osmotic flow profile in a nanochannel with double-layer overlap is almost parabolic and, as a result, it has been found that the effective electrophoretic transport rate for the counter-ions that reside close to the wall is decreased with respect to that of the co-ions in the middle of the channel[57,58]. Researchers have also observed electrophoretic separation of DNA oligomers (10–100 base pairs) in 100-nm-deep channels[59]. The observed dependence of the DNA transport rate on the ionic strength suggested an important role for the electrical double-layer field.

For pressure-driven flow, the transport rate of co-ions will be influenced by their charge number, because co-ions with higher charge number spend more time, on average, in the centre of the channel, where the flow rate is highest. Nanofluidics could therefore also have applications in ion separation[60]. Moreover, this effect
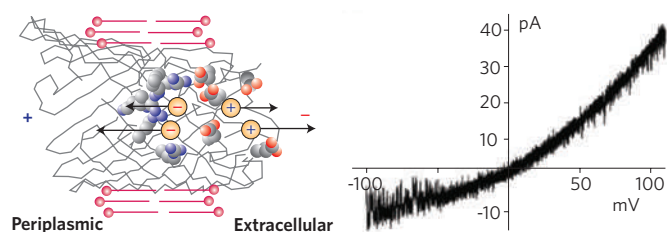
Figure 6 | A biological porin engineered into a nanofluidic diode.
Schematic showing a modified porin (grey) between bilipid membranes (red). The walls of the pore through the molecule are modified so that there are regions of positive (blue) and negative (red) charge. Since the electrical double layers are comparable with the diameter of the pore, a p–n junction that is equivalent to an electronic diode is created, as shown in the current–voltage curve on the right. Reprinted with permission from ref. 76 © 2007 ACS.

is thought to be responsible for the pressure-driven separation of DNA molecules recently observed in 500-nm-high channels[61].

The influence of steric exclusion. When the transport of solute through a nanochannel is exclusively determined by steric exclusion (that is, when friction and the hydrodynamic flow profile have negligible influence), the solute flux will only be a function of Φ (see equation (2)), and this coefficient was first calculated for different channel and solute shapes in 1968 (ref. 19). Researchers have developed nanostructured anisotropic sieves to perform Ogston sieving (named after Alexander George Ogston, who did pioneering work on the thermodynamics of biological systems in the 1950s; ref. 62) in a continuous flow fashion[63].

Steric exclusion confines larger solutes to the centre of the nanochannel, so they will be transported faster when a parabolic hydrodynamic flow profile exists. This process forms the basis of a size-dependent separation process called hydrodynamic chromatography that has been used to separate nanoparticles and biomolecules with sizes of order 10 nm (ref. 64), and also to separate DNA[65].

It can be difficult for non-spherical macromolecules to enter nanochannels because they are sterically excluded from part of the nanochannel and because they have to sacrifice rotational or conformational entropic freedom. As the energy required to overcome this entry barrier will depend on molecular size, this process can also form the basis for separation devices. A number of DNA separation devices use a succession of microcavities ('entropic traps') and nanochannels, where an interplay between conformational entropy and migration determines the separation order of long DNA[63,66]. Similar devices can also be used for the separation of short DNA molecules: because these molecules have a rigid rod conformation, the separation is based on differences in rotational entropy[67]. The tendency of DNA molecules to maximize their conformational entropy has been used for separation in entropic recoil devices[68]. However, the timescales for separation in these devices are long because diffusion is necessarily involved. Ref. 69 contains an eloquent discussion of entropy and separation.

The influence of friction. It has been repeatedly reported that the electrokinetic mobility of DNA in a nanochannel is lower than in bulk solution and several groups have demonstrated electrophoretic separation of DNA in nanochannels[70]. Some authors ascribe the separation to a size-dependent friction between the wall and the molecule, especially if extremely small channels are used. However, a simple friction model could only partly explain the observed decrease in DNA mobility in nanochannels that were 100 nm deep and 90 nm wide[71]. The separation of long (2–10 kilobase pairs) DNA molecules in nanoslits (channels that only have their height in the nanometre range) of 19 nm height was attributed to a differential friction with the walls[72].

Other researchers found that the mobility of long (2.8 and 48 kilobase pairs) DNA molecules in nanoslits of 20 nm height depended on the DNA length and also strongly on the applied field, with transient trapping observed at higher fields[73]. In view of the strength of the applied fields (up to 200 kV m^{-1}), dielectrophoresis and steric trapping were suggested as explanations. It must be mentioned that a short polymer (polyvinylpyrrolidone) was used in refs 71–73 to suppress electro-osmotic flow, and it is possible that this polymer could cause further friction and, possibly, a gel-type DNA separation.

Actively controlling transport. It is possible to control solute transport in nanochannels by modulating the electrostatic interactions between the solute molecules and the walls (similar to the methods used to control solvent transport). Examples of this approach applied to controlling the flow of ionic solutes include changing the pH to control transport through a membrane[74] and changing the electrolyte strength to gain control over the transport properties of a specifically engineered nanochannel[54].

The most promising and versatile technique involves the use of electrodes on the exterior of a nanochannel with thin walls (made of native silica) to actively vary the electrostatic potential at the wall to control the diffusional transport of charged proteins (Fig. 5; ref. 75). To limit the colloidal interactions to controllable electrostatic interactions, the wall of the nanochannel was modified to have a low surface charge while remaining strongly hydrophilic.

Transport through a biological porin can be controlled directly by altering the polarity of some of the surface groups inside the porin to create a nanofluidic diode (Fig. 6; ref. 76). External control of the rectifying properties of a comparable porin has also been demonstrated by altering the pH of the external solutions[77]. Similar control has been demonstrated for synthetic nanopores by functionalizing the nanopore with amphoteric surface groups[78].

A growing trend in nanofluidics is the development of the fluidic equivalents of well-known electrical circuit elements such as diodes[76–81,86] and transistors[75,82–85]. Inspired by the semiconductor, it may be possible to integrate these components into systems that could have applications in areas such as drug discovery[87].

Entrance and exit effects. Micromachining techniques have made it easy to manufacture systems in which nanochannels are interfaced to microchannels, and the entrance and exit effects (such as concentration polarization) at the ends of the nanochannels in these devices can be exploited in applications such as ion enrichment and ion depletion[88]. Other demonstrations have included the use of the ion-depletion zone in front of a nanochannel to preconcentrate proteins in a microchannel orthogonal to this nanochannel[89], and the simultaneous concentration and separation of an analyte in the depletion and enrichment zones[90–92].

Dealing with low detection limits. A drawback of nanofluidic separation systems is their low sample throughput, which gives rise to detection problems. (See ref. 6 for a discussion on molecular sensing in nanofluidic systems.) These problems can be approached in several ways. A continuous flow format can increase the amount of separated analyte, although the analysis time will increase[63,65,93,94]. Alternatively, concentration polarization can be used to preconcentrate analytes in an orthogonal microchannel[89]. Both these approaches rely on the ability of micromachining methods to fabricate devices with channels with heights and widths as small as 50 nm (ref. 95). Another possible approach is the use of parallel separation channels with parallel detection in each channel.

Energy conversion
We have seen that a streaming current and a streaming potential are generated by solvent flow through a charged nanochannel, and the possibility of using these phenomena to generate electrical energy

was explored theoretically in the 1960s (refs 96,97), but interest in these ideas later faded. However, advances in nanofabrication and worries about energy security have led researchers to revisit these ideas. The main challenge is to increase efficiency, which is at present around a few per cent[29–31,98–100], compared with efficiencies of up to about 95 per cent for standard rotational electromagnetic generators.

Theorists have recently discussed[29,100] ways to increase efficiency and implement parallelization. For systems without liquid slip the maximum achievable efficiency was predicted to be ~10%, which could be increased to ~30% if it were possible to take advantage of liquid slip to increase the flow. However, surfaces that facilitate slip are often hydrophobic and are known to have a lower effective surface charge, which would limit the efficiency. It might be possible to overcome this problem (by, for example, doping, surface modification or voltage biasing), but these solutions would, in turn, reduce the surface hydrophobicity and, therefore, the amount of slip. However, the prospects seem promising in view of the fact that slip-enhanced electro-osmotic flow has recently been experimentally observed[26], and the realization that the streaming potential is simply the experimental inverse of the electro-osmotic flow[101]. This technique holds great potential for increasing power density by exploiting the possibilities for massive parallelization within relatively small surface areas offered by nanofluidic systems.

It has also been calculated that a nanotube-based system could, by exploiting parallelization, generate kW m^{-2} power densities[29], although the practicality of this approach needs to be proved by experiment. Another challenge will be to make reliable electrical interfaces with nanofluidic generators because the Ag/AgCl reference electrodes used at present have a limited lifetime, especially when a large amount of current is passed.

Conclusion and outlook

Based on the progress that has been made over the past decade, we expect that nanofluidic systems will have an important role in the following fields: analytical chemistry and biochemistry; liquid transport and metering; and energy conversion (especially if liquid slip can be exploited). The biggest challenge facing workers in the field is to cope with the inherent problems introduced by the enormous surface-to-volume ratios. Adsorption of molecules, for example, can lead to large losses and can also change the surface properties. Furthermore, detection issues will have to be dealt with in view of the very small quantities of molecules present.

References

1. Turner, S. W., Perez, A. M., Lopez, A. & Craighead, H. G. Monolithic nanofluid sieving structures for DNA manipulation. *J. Vac. Sci. Technol. B* **16,** 3835–3840 (1998).
2. Eijkel, J. C. T. & van den Berg, A. Nanofluidics: what is it and what can we expect from it? *Microfluid. Nanofluid.* **1,** 249–267 (2005).
3. Abgrall, P. & Nguyen, N. T. Nanofluidic devices and their applications. *Anal. Chem.* **80,** 2326–2341 (2008).
4. Mijatovic, D., Eijkel, J. C. T. & van den Berg, A. Technologies for nanofluidic systems: top-down vs. bottom-up — a review. *Lab Chip* **5,** 492–500 (2005).
5. Perry, J. L. & Kandlikar, S. G. Review of fabrication of nanochannels for single phase liquid flow. *Microfluid. Nanofluid.* **2,** 185–193 (2006).
6. Schoch, R. B., Han, J. Y. & Renaud, P. Transport phenomena in nanofluidics. *Rev. Mod. Phys.* **80,** 839–883 (2008).
7. Yuan, Z., Garcia, A. L., Lopez, G. P. & Petsev, D. N. Electrokinetic transport and separations in fluidic nanochannels. *Electrophoresis* **28,** 595–610 (2007).
8. Succi, S., Mohammad, A. A. & Horbach, J. Lattice-Boltzmann simulation of dense nanoflows: A comparison with molecular dynamics and Navier-Stokes solutions. *Int. J. Mod. Phys. C* **18,** 667–675 (2007).
9. Wijmans, J. G. & Baker, R. W. The solution-diffusion model — a review. *J. Membr. Sci.* **107,** 1–21 (1995).
10. Gad-el-Hak, M. The fluid mechanics of microdevices — The Freeman scholar lecture. *J. Fluid Eng.-T. ASME* **121,** 5–33 (1999).
11. Deen, W. M. Hindered transport of large molecules in liquid-filled pores. *AIChE J.* **33,** 1409–1425 (1987).
12. Prieve, D. C. & Hoysan, P. M. Role of colloidal forces in hydrodynamic chromatography. *J. Colloid Interf. Sci.* **64,** 201–213 (1978).
13. Ruckenstein, E. & Prieve, D. C. Adsorption and desorption of particles and their chromatographic separation. *AIChE J.* **22,** 276–283 (1976).
14. Bowen, W. R. & Mukhtar, H. Characterisation and prediction of separation performance of nanofiltration membranes. *J. Membr. Sci.* **112,** 263–274 (1996).
15. Lyklema, J. *Fundamentals of Interface and Colloid Science, Fundamentals* 1st edn (Academic Press, 2000).
16. Christenson, H. K. & Claesson, P. M. Direct measurements of the force between hydrophobic surfaces in water. *Ad. Colloid Interf. Sci.* **91,** 391–436 (2001).
17. Meyer, E. E., Rosenberg, K. J. & Israelachvili, J. Recent progress in understanding hydrophobic interactions. *Proc. Natl Acad. Sci. USA* **103,** 15739–15746 (2006).
18. Norde, W. in *Physical Chemistry of Biological Interfaces* (ed. Dekker, M.) 115–136 (CRC, 2000).
19. Giddings, J. C., Kucera, E., Russell, C. P. & Myers, M. N. Statistical theory for equilibrium distribution of rigid molecules in inert porous networks. Exclusion chromatography. *J. Phys. Chem.* **72,** 4397–4408 (1968).
20. Teraoka, I. Polymer solutions in confining geometries. *Prog. Polym. Sci.* **21,** 89–149 (1996).
21. Burgreen, D. & Nakache, F. R. Electrokinetic flow in ultrafine capillary slits. *J. Phys. Chem.* **68,** 1084–1091 (1964).
22. Levine, S., Marriott, J. R., Neale, G. & Epstein, N. Theory of electrokinetic flow in fine cylindrical capillaries at high zeta-potentials. *J. Colloid Interf. Sci.* **52,** 136–149 (1975).
23. Vinogradova, O. I. Slippage of water over hydrophobic surfaces. *Int. J. Miner. Process.* **56,** 31–60 (1999).
24. Cottin-Bizonne, C., Cross, B., Steinberger, A. & Charlaix, E. Boundary slip on smooth hydrophobic surfaces: Intrinsic effects and possible artefacts. *Phys. Rev. Lett.* **94,** 056102 (2005).
25. Muller, V. M., Sergeeva, I. P., Sobolev, V. D. & Churaev, N. V. Boundary effects in the theory of electrokinetic phenomena. *Colloid J. USSR* **48,** 606–614 (1986).
26. Bouzigues, C. I., Tabeling, P. & Bocquet, L. Nanofluidics in the Debye layer at hydrophilic and hydrophobic surfaces. *Phys. Rev. Lett.* **101,** 114503 (2008).
27. Joly, L., Ybert, C., Trizac, E. & Bocquet, L. Liquid friction on charged surfaces: From hydrodynamic slippage to electrokinetics. *J. Chem. Phys.* **125,** 204716 (2006).
28. Vermesh, U. *et al.* Fast nonlinear ion transport via field-induced hydrodynamic slip in sub-20-nm hydrophilic nanofluidic transistors. *Nano Lett.* **9,** 1315–1319 (2009).
29. Ren, Y. Q. & Stein, D. Slip-enhanced electrokinetic energy conversion in nanofluidic channels. *Nanotechnology* **19,** 195707 (2008).
30. van der Heyden, F. H. J., Bonthuis, D. J., Stein, D., Meyer, C. & Dekker, C. Power generation by pressure-driven transport of ions in nanofluidic channels. *Nano Lett.* **7,** 1022–1025 (2007).
31. Daiguji, H., Yang, P. D., Szeri, A. J. & Majumdar, A. Electrochemomechanical energy conversion in nanofluidic channels. *Nano Lett.* **4,** 2315–2321 (2004).
32. Stein, D., van der Heyden, F. H. J., Koopmans, W. J. A. & Dekker, C. Pressure-driven transport of confined DNA polymers in fluidic channels. *Proc. Natl Acad. Sci USA* **103,** 15853–15858 (2006).
33. Holt, J. K. *et al.* Fast mass transport through sub-2-nanometer carbon nanotubes. *Science* **312,** 1034–1037 (2006).
34. Majumder, M., Chopra, N., Andrews, R. & Hinds, B. J. Nanoscale hydrodynamics: Enhanced flow in carbon nanotubes. *Nature* **438,** 44–44 (2005).
35. Eijkel, J. C. T., Bomer, J. G. & van den Berg, A. Osmosis and pervaporation in polyimide submicron microfluidic channel structures. *Appl. Phys. Lett.* **87,** 114103 (2005).
36. Karlsson, R. *et al.* Moving-wall-driven flows in nanofluidic systems. *Langmuir* **18,** 4186–4190 (2002).
37. Soare, M. A., Picu, R. C., Tichy, J., Lu, T. M. & Wang, G. C. Fluid transport through nanochannels using nanoelectromechanical actuators. *J. Intell. Mater. Sys. Struct.* **17,** 231–238 (2006).
38. Tas, N. R., Berenschot, J. W., Lammerink, T. S. J., Elwenspoek, M. & van den Berg, A. Nanofluidic bubble pump using surface tension directed gas injection. *Anal. Chem.* **74,** 2224–2227 (2002).
39. Prieve, D. C., Anderson, J. L., Ebel, J. P. & Lowell, M. E. Motion of a particle generated by chemical gradients. 2. Electrolytes. *J. Fluid Mech.* **148,** 247–269 (1984).
40. Anderson, J. L., Prieve, D. C. & Ebel, J. P. Chemically induced migration of particles across fluid streamlines. *Chem. Eng. Commun.* **55,** 211–224 (1987).
41. Keh, H. J. & Wei, Y. K. Diffusioosmosis and electroosmosis of electrolyte solutions in fibrous porous media. *J. Colloid Interf. Sci.* **252,** 354–364 (2002).
42. Qian, S. Z., Das, B. & Luo, X. B. Diffusioosmotic flows in slit nanochannels. *J. Colloid Interf. Sci.* **315,** 721–730 (2007).
43. Ajdari, A. & Bocquet, L. Giant amplification of interfacially driven transport by hydrodynamic slip: Diffusio-osmosis and beyond. *Phys. Rev. Lett.* **96,** 186102 (2006).

44. Goedecke, N., Eijkel, J. & Manz, A. Evaporation driven pumping for chromatography application. *Lab Chip* **2,** 219–223 (2002).
45. Wheeler, T. D. & Stroock, A. D. The transpiration of water at negative pressures in a synthetic tree. *Nature* **455,** 208–212 (2008).
46. Huh, D. *et al.* Tuneable elastomeric nanochannels for nanofluidic manipulation. *Nature Mater.* **6,** 424–428 (2007).
47. Quake, S. R. & Scherer, A. From micro- to nanofabrication with soft materials. *Science* **290,** 1536–1540 (2000).
48. Poppe, H. Some reflections on speed and efficiency of modern chromatographic methods. *J. Chromatogr. A* **778,** 3–21 (1997).
49. Kievsky, Y. Y. *et al.* Dynamics of molecular diffusion of rhodamine 6G in silica nanochannels. *J. Chem. Phys.* **128,** 151102 (2008).
50. Durand, N. F. Y., Bertsch, A., Todorova, M. & Renaud, P. Direct measurement of effective diffusion coefficients in nanochannels using steady-state dispersion effects. *Appl. Phys. Lett.* **91,** 203106 (2007).
51. Karnik, R., Castelino, K., Duan, C. H. & Majumdar, A. Diffusion-limited patterning of molecules in nanofluidic channels. *Nano Lett.* **6,** 1735–1740 (2006).
52. Yamaguchi, A. *et al.* Diffusion of metal complexes inside silica-surfactant nanochannels within a porous alumina membrane. *J. Phys. Chem. B* **112,** 2024–2030 (2008).
53. Yamaguchi, A., Yoda, T., Suzuki, S., Morita, K. & Teramae, N. Diffusivities of tris(2,2′-bipyridyl)ruthenium inside silica-nanochannels modified with alkylsilanes. *Anal. Sci.* **22,** 1501–1507 (2006).
54. Schoch, R. B., Bertsch, A. & Renaud, P. pH-controlled diffusion of proteins with different pI values across a nanochannel on a chip. *Nano Lett.* **6,** 543–547 (2006).
55. Crank, J. *The Mathematics of Diffusion* (Oxford Univ. Press, 1975).
56. Delamarche, E., Bernard, A., Schmid, H., Michel, B. & Biebuyck, H. Patterned delivery of immunoglobulins to surfaces using microfluidic networks. *Science* **276,** 779–781 (1997).
57. Pennathur, S. & Santiago, J. G. Electrokinetic transport in nanochannels. 1. Theory. *Anal. Chem.* **77,** 6772–6781 (2005).
58. Pennathur, S. & Santiago, J. G. Electrokinetic transport in nanochannels. 2. Experiments. *Anal. Chem.* **77,** 6782–6789 (2005).
59. Pennathur, S. *et al.* Free-solution oligonucleotide separation in nanoscale channels. *Anal. Chem.* **79,** 8316–8322 (2007).
60. Xuan, X. C. Ion separation in nanofluidics. *Electrophoresis* **29,** 3737–3743 (2008).
61. Wang, X. Y., Kang, J. Z., Wang, S. L., Lu, J. J. & Liu, S. R. Chromatographic separations in a nanocapillary under pressure-driven conditions. *J. Chromatogr. A* **1200,** 108–113 (2008).
62. Ogston, A. G. The spaces in a uniform random suspension of fibres. *Trans. Faraday Soc.* **54,** 1754–1757 (1958).
63. Fu, J. P., Schoch, R. B., Stevens, A. L., Tannenbaum, S. R. & Han, J. Y. A patterned anisotropic nanofluidic sieving structure for continuous-flow separation of DNA and proteins. *Nature Nanotech.* **2,** 121–128 (2007).
64. Blom, M. T., Chmela, E., Oosterbroek, R. E., Tijssen, R. & van den Berg, A. On-chip hydrodynamic chromatography separation and detection of nanoparticles and biomolecules. *Anal. Chem.* **75,** 6761–6768 (2003).
65. Stein, D., van der Heyden, F. H. J., Koopmans, W. J. A. & Dekker, C. Pressure driven transport of confined DNA polymers in fluidic channels. *Proc. Natl Acad. Sci. USA* **103,** 15853–15858 (2006).
66. Han, J. & Craighead, H. G. Separation of long DNA molecules in a microfabricated entropic trap array. *Science* **288,** 1026–1029 (2000).
67. Li, Z. R. *et al.* Continuum transport model of Ogston sieving in patterned nanofilter arrays for separation of rod-like biomolecules. *Electrophoresis* **29,** 329–339 (2008).
68. Turner, S. W. P., Cabodi, M. & Craighead, H. G. Confinement-induced entropic recoil of single DNA molecules in a nanofluidic structure. *Phys. Rev. Lett.* **88,** 128103 (2002).
69. Austin, R. Nanofluidics: A fork in the nano-road. *Nature Nanotech.* **2,** 79–80 (2007).
70. Tegenfeldt, J. O. *et al.* Micro- and nanofluidics for DNA analysis. *Anal. Bioanal. Chem.* **378,** 1678–1692 (2004).
71. Mannion, J. T., Reccius, C. H., Cross, J. D. & Craighead, H. G. Conformational analysis of single DNA molecules undergoing entropically induced motion in nanochannels. *Biophys. J.* **90,** 4538–4545 (2006).
72. Cross, J. D., Strychalski, E. A. & Craighead, H. G. Size-dependent DNA mobility in nanochannels. *J. Appl. Phys.* **102,** 024514 (2007).
73. Salieb-Beugelaar, G. B. *et al.* Field-dependent DNA mobility in 20 nm high nanoslits. *Nano Lett.* **8,** 1785–1790 (2008).
74. Kuo, T. C., Sloan, L. A., Sweedler, J. V. & Bohn, P. W. Manipulating molecular transport through nanoporous membranes by control of electrokinetic flow: Effect of surface charge density and Debye length. *Langmuir* **17,** 6298–6303 (2001).
75. Karnik, R., Castelino, K. & Majumdar, A. Field-effect control of protein transport in a nanofluidic transistor circuit. *Appl. Phys. Lett.* **88,** 123114 (2006).
76. Miedema, H. *et al.* A biological porin engineered into a molecular, nanofluidic diode. *Nano Lett.* **7,** 2886–2891 (2007).
77. Garcia-Gimenez, E., Alcaraz, A., Aguilella, V. M. & Ramirez, P. Directional ion selectivity in a biological nanopore with bipolar structure. *J. Membr. Sci.* **331,** 137–142 (2009).
78. Ali, M., Ramirez, P., Mafe, S., Neumann, R. & Ensinger, W. A pH-tunable nanofluidic diode with a broad range of rectifying properties. *ACS Nano* **3,** 603–608 (2009).
79. Karnik, R., Duan, C. H., Castelino, K., Daiguji, H. & Majumdar, A. Rectification of ionic current in a nanofluidic diode. *Nano Lett.* **7,** 547–551 (2007).
80. Alcaraz, A. *et al.* A pH-tunable nanofluidic diode: Electrochemical rectification in a reconstituted single ion channel. *J. Phys. Chem. B* **110,** 21205–21209 (2006).
81. Cheng, L. J. & Guo, L. J. Rectified ion transport through concentration gradient in homogeneous silica nanochannels. *Nano Lett.* **7,** 3165–3171 (2007).
82. Fan, R., Huh, S., Yan, R., Arnold, J. & Yang, P. D. Gated proton transport in aligned mesoporous silica films. *Nature Mater.* **7,** 303–307 (2008).
83. Fan, R., Yue, M., Karnik, R., Majumdar, A. & Yang, P. D. Polarity switching and transient responses in single nanotube nanofluidic transistors. *Phys. Rev. Lett.* **95,** 086607 (2005).
84. Karnik, R. *et al.* Electrostatic control of ions and molecules in nanofluidic transistors. *Nano Lett.* **5,** 943–948 (2005).
85. Kuo, T. C. *et al.* Gateable nanofluidic interconnects for multilayered microfluidic separation systems. *Anal. Chem.* **75,** 1861–1867 (2003).
86. Vlassiouk, I. & Siwy, Z. S. Nanofluidic diode. *Nano Lett.* **7,** 552–556 (2007).
87. Gijs, M. A. M. Device physics: Will fluidic electronics take off? *Nature Nanotech.* **2,** 268–270 (2007).
88. Pu, Q. S., Yun, J. S., Temkin, H. & Liu, S. R. Ion-enrichment and ion-depletion effect of nanochannel structures. *Nano Lett.* **4,** 1099–1103 (2004).
89. Wang, Y. C., Stevens, A. L. & Han, J. Y. Million-fold preconcentration of proteins and peptides by nanofluidic filter. *Anal. Chem.* **77,** 4293–4299 (2005).
90. Mani, A., Zangle, T. A. & Santiago, J. G. On the propagation of concentration polarization from microchannel-nanochannel interfaces part I: Analytical model and characteristic analysis. *Langmuir* **25,** 3898–3908 (2009).
91. Zangle, T. A., Mani, A. & Santiago, J. G. On the propagation of concentration polarization from microchannel-nanochannel interfaces part II: Numerical and experimental study. *Langmuir* **25,** 3909–3916 (2009).
92. Plecis, A., Nanteuil, C., Haghiri-Gosnet, A. M. & Chen, Y. Electropreconcentration with charge-selective nanochannels. *Anal. Chem.* **80,** 9542–9550 (2008).
93. Han, A. P., de Rooij, N. F. & Staufer, U. Design and fabrication of nanofluidic devices by surface micromachining. *Nanotechnology* **17,** 2498–2503 (2006).
94. Han, J. Y., Fu, J. P. & Schoch, R. B. Molecular sieving using nanofilters: Past, present and future. *Lab Chip* **8,** 23–33 (2008).
95. Eijkel, J. C. T. Scaling revisited. *Lab Chip* **7,** 1630–1632 (2007).
96. Osterle, J. F. Unified treatment of thermodynamics of steady-state energy conversion. *Appl. Sci. Res. A* **12,** 425–434 (1964).
97. Burgreen, D. & Nakache, F. R. Efficiency of pumping and power generation in ultrafine electrokinetic systems *J. Appl. Mech.* **32,** 675–679 (1965).
98. Davidson, C. & Xuan, X. C. Electrokinetic energy conversion in slip nanochannels. *J. Power Sources* **179,** 297–300 (2008).
99. Davidson, C. & Xuan, X. C. Effects of Stern layer conductance on electrokinetic energy conversion in nanofluidic channels. *Electrophoresis* **29,** 1125–1130 (2008).
100. Pennathur, S., Eijkel, J. C. T. & van den Berg, A. Energy conversion in microsystems: is there a role for micro/nanofluidics? *Lab Chip* **7,** 1234–1237 (2007).
101. Probstein, R. F. *Physicochemical Hydrodynamics: An Introduction* 2nd edn (Wiley, 1994).
102. van Oss, C. J. Long-range and short-range mechanisms of hydrophobic attraction and hydrophilic repulsion in specific and aspecific interactions. *J. Mol. Recogn.* **16,** 177–190 (2003).
103. Ninham, B. W. & Yaminsky, V. Ion binding and ion specificity: The Hofmeister effect and Onsager and Lifshitz theories. *Langmuir* **13,** 2097–2108 (1997).
104. Pierret, R. F. *Semiconductor Device Fundamentals* (Addison-Wesley, 1996).

Acknowledgements